Hindawi
Shock and Vibration
Volume 2024, Article ID 9285252, 16 pages
https://doi.org/10.1155/2024/9285252

Research Article

Study on Numerical Simulation of Surrounding Rock Structure Safety of Urban Underwater Shield Tunnel: A Case in Chongqing

Zeng-Qiang Yang,[1,2] **Xiao-Ming You**,[3] **and Hui-Wu Jin**[1]

[1]*School of Transportation Engineering, Jiangsu Vocational Institute of Architectural Technology, Xuzhou, Jiangsu 221116, China*
[2]*Xuzhou Coal Mining Group Corporation Ltd, Xuzhou, Jiangsu 221018, China*
[3]*Chongqing Vocational Institute of Engineering, Chongqing 402260, China*

Correspondence should be addressed to Zeng-Qiang Yang; zengqiang5@126.com

Received 17 October 2022; Revised 20 December 2023; Accepted 30 December 2023; Published 17 January 2024

Academic Editor: Andrzej Katunin

Based on the engineering background of shield construction of a subway section in Chongqing, which needs to pass through a park and there is a lake inside this park, this paper adopts theoretical analysis methods and numerical simulation calculation methods to explore the distribution law of the seepage field and the characteristics of water pressure in lining segments during shield tunneling. The results show that, during the whole excavation of a double-track tunnel with EPB shield, the maximum vertical effective stress is about 4.24 MPa, which is located at the arch foot of the tunnel. The maximum effective stress in the horizontal direction is about 3.61 MPa, which is located on both side walls of the tunnel in the horizontal direction; after the left and right tunnels are excavated in sequence, a "double precipitation funnel-shaped" pore pressure distribution is formed around the tunnel; during the construction of the shield tunnel, the vertical displacement and horizontal displacement of the surrounding rock show an increasing trend and gradually tend to be stable values of 24.09 mm and 25.28 mm; the segment vault has settlement, the maximum settlement is 21.8 mm, the arch bottom has uplift, and the maximum uplift is 24.4 mm. The maximum horizontal displacement of the segment appears on both sides of the arch waist, and the maximum horizontal displacement decreases with the increase of excavation steps; the positive bending moment of the lining segment is mainly distributed on both sides of the arch crown, and the negative bending moment is mainly distributed on both sides of the arch bottom. The axial force of the lining segment is compressive stress, and the maximum axial force is mainly distributed on both sides of the arch waist. The maximum normal shear stress occurs on both sides of the segment arch bottom. The study conclusions provide theoretical foundation and a new guidance for long-term safety evaluation of underwater tunnel structures.

1. Introduction

At present, there are mainly three kinds of transportation modes available at home and abroad for crossing rivers, lakes, and seas: bridges, ferries, and underwater tunnels. With the rapid development of China's economy and urban construction, the improvement of underwater tunnel construction technology, and the enhancement of people's environmental awareness, urban underwater tunnels have become the preferred mode of transportation across rivers, lakes, and seas [1–3]. At present, the large tunnel projects that have been built and are under construction in China include the Xiamen Xiang'an Submarine Tunnel, Qingdao Jiaozhou Bay Submarine Tunnel, Nanchang Honggu Tunnel, Wuhan Yangtze River Tunnel, Suzhou Dushu Lake Tunnel, and Changzhou Wuxi Taihu Lake Tunnel. It can be seen that the urban underwater tunnel has a good application and development prospect in China [4–6].

Internationally, from the Green Heart Tunnel in the Netherlands, there have been M30 Road Tunnel in Madrid, Spain, SPARVO Tunnel in Italy, and Alaska Way Tunnel in Seattle, the United States, and other super diameter tunnel projects. In China, the Jinan Yellow River Tunnel, which started in December 2017, is the largest diameter shield tunnel under construction in China, with a shield diameter of 15.2 m. Shield tunneling is a fully mechanized

construction method that is widely used in the construction of underground excavation method, and has a relatively mature technical system [7, 8]. During the construction process, the shield machine uses the shield shell and precast concrete segments to support surrounding rocks while advancing underground to prevent the collapse of the tunnel inner wall, thus forming the tunnel structure. The urban underwater tunnel is mainly composed of the upper lining and the lower subgrade. When the underwater tunnel is constructed by the shield method, especially the super diameter underwater tunnel constructed to meet the increasing traffic demand, the challenge of the complex geological environment of the underwater stratum and large-scale structure in the construction process is much more difficult than the conventional shield tunnel construction. During the construction of supe-large diameter underwater tunnel with shield method, the surrounding rock of the tunnel will be more seriously affected [9, 10]. For example, the interaction of mud and water, the fluid-solid coupling effect, shield tail grouting, and concrete segment wall thickness grouting during the shield construction will affect the shaping quality after the tunnel shield construction. When the shield construction is completed, the excellent coordination between the surrounding rock and structure of the formed super-large diameter underwater shield tunnel will directly have an important impact on the safety of the tunnel in the subsequent long-term service period. For example, the surrounding rock structure of the formed tunnel will be safe under the influence of geological tectonic stress, water pressure, corrosive water environment, and traffic load disturbance in the subsequent long-term service period. It will directly affect the service life of the tunnel and the safety of vehicles and other means of transportation [11–13].

With the continuous expansion of the diameter and length of urban underwater shield tunnels, the construction conditions and difficulties of typical tunnels in different locations are different. The subjective evaluation of the construction quality of a large underwater shield tunnel is mainly determined by the development of shield technology and the organization and management regulations during the shield construction process. The objective evaluation of the formed large underwater shield tunnel needs to be analyzed from the perspective of whether the surrounding rock structure design of the tunnel is reasonable and whether it can meet the long-term safety requirements during the service period. How to evaluate and ensure the rationality and long-term safety of the surrounding rock structure design of large underwater shield tunnels has become one of the key problems to be solved urgently for the safe operation of large underwater shield tunnels in our province and even in the country.

2. The Development Status of Urban Underwater Tunnel

China has a vast territory with a large distribution of rivers, lakes, and sea waters. The area of inland waters including the seven major river systems of the Yangtze River, Yellow River, Huaihe River, and Haihe River reaches 174700 km^2; including more than 5000 rivers with a drainage area of more than 100 km^2, and the total area of natural lakes above 1 km^2 is about 80000 km^2. In addition, there are Liaodong Bay, Bohai Bay, Laizhou Bay, Hangzhou Bay, Beibu Bay, and other bays with a water area of more than 5000 km^2. It can be seen that on the vast land of China, while rivers, lakes, and seas bring people rich water resources, they will also naturally divide geographical units. With the significant improvement of the development level of global economic integration, the factor flow and resource integration between different regional economic units are becoming more and more frequent. Therefore, it is urgent to improve the traffic barrier between urban blocks, cities, regions, and international waters caused by rivers and lakes [14–17].

With the rapid development of the economy and the great progress of science and technology, underwater tunnel construction technology has also made great progress. At present, underwater tunnel has gradually become an important means of transportation across rivers, lakes, and seas at home and abroad. Especially, it has become an important alternative in the construction of cross-river and cross-sea traffic projects such as railways, highways, and urban subways [18]. The construction methods of underwater tunnels mainly include mining method, pipe sinking method, and shield method. In actual projects, specific construction methods are selected according to the geological conditions of tunnel engineering. Generally speaking, the mining method is mainly applicable to the medium-hard rock stratum with good integrity, which has a large disturbance to the surrounding rock of the tunnel, often requires a variety of auxiliary construction methods to cooperate, and has a poor ability to deal with water inrush. The immersed pipe method is limited by many factors such as water flow velocity, water temperature, climate, and weather, and its application and popularity are not high. Shield tunneling has become an important construction method for underwater tunnel construction because it is not affected by rivers, seasons, and other conditions and has the advantages of a small impact on the surrounding environment, strong adaptability to complex geological structure conditions, and safe and fast construction.

Different from other tunnels, the geological conditions and internal and external environment of underwater tunnels are generally complex. If disasters occur during the operation period, it is easy to cause significant economic losses and adverse social impacts. Investigation and research at home and abroad show that a high proportion of tunnels have lining cracks and water leakage, which affect traffic quality, threaten driving safety, and shorten the maintenance cycle and service life of tunnels. At present, the total number and length of tunnels built in China rank first in the world. However, due to engineering geological conditions, design, construction, operation, maintenance, and management, the problem of tunnel diseases is very serious. According to incomplete statistics, out of 5800 officially operated tunnels in China, 3671 are diseased, accounting for 63.3%. The main disease types are tunnel seepage, lining crack, lining corrosion, earthquake damage, air pollution in the tunnel, and

fire. Because the large or super-large underwater shield tunnel structure section is often huge, the stress characteristics of the main structure of tunnel segment lining are extremely complex. This kind of tunnel is located in a relatively complex engineering geological background of rivers, lakes, and sea bottom, which has the characteristics of high water pressure, strong permeability, and complex underwater environment, and is in the underwater erosion environment for a long time, which has a great impact on the durability of the structure. At the same time, during the subsequent operation of such tunnels, the plastic deformation of soil mass caused by traffic cyclic load will cause uneven settlement along the longitudinal and transverse direction of the tunnel. It can be seen that the structural stability and durability of underwater tunnels are the key theories and technologies that need to be studied in the design, construction, and operation stages. However, China started large-scale construction of transportation infrastructure only in the 1980s, and the research on long-term safety of underwater tunnels started late in China. With the operation of a large number of super-large diameter underwater tunnels in recent years, the research on the mechanism of underwater tunnel structural disease and its prevention has become extremely urgent [19–21].

Therefore, it is necessary to deeply study the safety evolution mechanism of large underwater tunnel structures during long-term operation, establish long-term safety evaluation and analysis methods and safety early warning strategies for underwater tunnel structures, and provide guidance for timely taking corresponding technical support measures to reduce disasters and adverse effects caused by tunnel structural diseases. It has important scientific significance and application value for promoting the development of underwater tunnel structure in our province and even the whole country and the infrastructure construction of the "Belt and Road."

3. The Coupling Theory Analysis of Seepage Field and Stress Field

Shield tunneling is one of the most advanced construction methods for crossing rivers, lakes, and seas. Its advantages such as fast construction, high quality and efficiency, safety, environmental protection, and high automation and informatization make shield tunneling more and more valued and favored. However, during the construction and later operation of the underwater shield tunnel, due to the high underground water pressure and the influence of a stable recharge water source, the seepage problem during the construction and later operation of underwater shield tunnel is particularly prominent. The major water inrush accidents that occurred during the construction of the Old Dana Tunnel, the Denmark Strait Submarine Tunnel, the Tianjin Metro Line 6 Tunnel, and the Maluqing Tunnel on the Tokaido Trunk Line in Japan have seriously affected the stability and construction period of the tunnels.

During the construction of the shield tunnel, the soil around the tunnel will be disturbed to varying degrees, resulting in varying degrees of deformation of the soil, resulting in changes in the physical and mechanical characteristics of the soil, especially changes in the permeability, which will lead to changes in the groundwater seepage field. At the same time, the change of groundwater seepage field will also affect the stress state of soil mass, making the stress field redistribute. The two interact and influence each other, which leads to the fluid-solid coupling problem in the shield tunnel construction process.

Considering that the FLAC^{3D} software can perform fluid calculations separately, only considering the effect of seepage, or coupling fluid calculations with mechanical calculations, commonly known as fluid structure coupling calculations, it is necessary to preliminarily determine its relevant parameters.

Assume that the initial porosity of soil mass can be expressed as follows:

$$n_o = 1 - \frac{V_s}{V_o}, \tag{1}$$

where V_o is the initial total volume of soil mass, m^3, and V_s is the total volume of soil mass after deformation, m^3.

Assuming that the soil particles are incompressible, the soil porosity after deformation can be expressed as follows:

$$n = 1 - \frac{V_s}{V}, \tag{2}$$

where V is the total volume of soil mass after deformation, m^3.

For the problem under small strain, the volume strain can be expressed as follows:

$$\varepsilon_v = \frac{V - V_o}{V_o}. \tag{3}$$

By comparing equations (1) –(3), the following expression can be deduced:

$$n = \frac{n_o + \varepsilon_v}{1 + \varepsilon_v}. \tag{4}$$

Based on the plane strain theory, it is known that $\varepsilon_z = 0$, therefore the corresponding volumetric strain can be expressed as follows:

$$\varepsilon_v = \varepsilon_r + \varepsilon_\theta. \tag{5}$$

According to the constitutive equation [22, 23],

$$\begin{cases} \varepsilon_r = \dfrac{1}{E_c'}\left(\sigma_r - \nu_c' \cdot \varepsilon_\theta\right), \\ \varepsilon_\theta = \dfrac{1}{E_c'}\left(\sigma_\theta - \nu_c' \cdot \varepsilon_r\right), \end{cases} \tag{6}$$

where $E_c' = E_c/1 - \nu_c'$ and $\nu_c' = \nu_c/1 - \nu_c$.

Substituting equation (4) into the Kozeny–Carman equation in seepage mechanics to obtain the fluid-solid coupling equation,

$$K = \frac{K_o}{(1+\varepsilon_v)^3} \cdot \left(1 + \frac{\varepsilon_v}{n_o}\right)^3, \quad (7)$$

where K_o is the initial permeability coefficient; n_o is the initial porosity; and ε_v is the volumetric strain.

Based on the coupling theory of seepage field and stress field, the equations of seepage field and stress field coupling are derived, which provides theoretical support for the follow-up research on the fluid structure coupling problem of the underwater shield tunnel and numerical simulation. In the future, the relevant equations of seepage stress field coupling can be embedded into the FLAC^{3D} software for simulation operations by combining the FISH program. The seepage mode has been selected in the FLAC^{3D} software, which is to set the "CONFIG fluid" command in the calculation.

4. The Numerical Simulation of Seepage Field

4.1. The Engineering Background of Shield Construction. The engineering background of shield construction is based on the construction of a subway section in Chongqing. The design mileage of this subway section includes two lines, and they are left line and right line, respectively. The specific parameters of left and right lines are as follows: the design mileage of left section is ZCK22 + 018.113~ZCK23 + 116.583, and its total length is about 1098.883 m; the design mileage of right section is YCK22 + 017.313~YCK23 + 194.383, and its total length is about 1176.270 m; the left line and right line are almost parallel, and the space between them is about 14.2~18.2 m; the thickness of overburden soil above this subway section is about 10.8~24.5 m.

This subway section needs to pass through a park, and there is a lake inside this park. The length of this subway section passing through the bottom of this lake is about 156.0 m, which puts forward higher requirements for the safe construction of this special subway section and long-term safe operation in the later period. This special subway section under the influence of lake is constructed by earth pressure balance (EPB) shield method, and its starting and ending mileages are ZCK22 + 695.00~ZCK22 + 851.00 (left line) and YCK22 + 695.00~YCK22 + 851.00 (right line). The length of left line is about 148.0 m, and the length of right line is about 162.0 m. The average space (L) between left line and right line in special subway section is about 14.2 m. The average buried depth (H) of left and right lines in special subway section is about 18.0 m, and the depth of this lake is about 5.0 m. The tunnel lining segment is standard single round and made of C50 concrete, and its thickness and width are 350 mm and 1.2 m, respectively. The outer diameter (D) and inner diameter (d) of this tunnel are 6200 and 5500 mm, respectively. The cross-section sketch of a special subway section passing through a lake is shown in Figure 1.

Therefore, this special subway section passing through the lake is selected for numerical simulation research and analysis. Considering that the tunnel lining segment width for both left line and right line is about 1.2 m, so the shield driving length of 1.2 m can be selected as a numerical simulation excavation step. The left and right lines are excavated asynchronously. The left line is excavated in 1~130 steps, and the right line is excavated in 131~260 steps. A total of 260 excavation steps are completed, finally. Three typical cross-sections are selected during the whole shield driving process for research and analysis of numerical simulation results, and they are as follows: the shield tunneling machine has just penetrated the bottom of this lake (mileage: YCK22 + 701.00), the shield machine goes through the middle of the bottom of this lake (mileage: YCK22 + 773.00), and the shield machine is about to leave the bottom of this lake (mileage: YCK22 + 845.00). The plan sketch of special subway section passing through a lake is shown in Figure 2.

According to Figure 2, it can be seen that the lake will seep into the soil below the lakebed, and the drilling hole for engineering investigation shows that the special subway section is within the influence range of slightly confined water. Therefore, the underground seepage will have a great effect on the construction of the left and right lines.

4.2. The Establishment of Three-Dimensional Model. In order to reduce the influence of the boundary effect and considering that the soil is an infinite body, the range of soil stress redistribution after tunnel excavation is 3~5 times of the tunnel diameter in the horizontal direction, so the calculation range of this three-dimensional model is as follows: the upper part is the actual thickness of the overlying rock and soil layer, that is, the distance from the lakebed to the top of the tunnel. The final dimensions of the constructed 3D model are 156 m (long) × 77 m (wide) × 46 m (height). The model is divided into 237640 units and 244332 nodes. The Mohr–Coulomb elastoplastic model is used for each soil layer and grouting layer unit, and the shell unit is used for tunnel lining segments. Finally, the established three-dimensional model is shown in Figure 3.

According to the geological investigation report and analogy of similar projects [24], the density of the tunnel lining segment is 253 kN/m, the elastic modulus is 3.7×10^4 MPa, and Poisson's ratio is 0.17 in the numerical simulation calculation process; the density of the grouting body is 243 kN/m, the elastic modulus is 4.0 MPa, the cohesion is 15.0 kPa, Poisson's ratio is 0.31, and the internal friction angle is 25°. The physical and mechanical parameters of soil mass in each layer are shown in Table 1.

The boundary conditions of this three-dimensional model are as follows: the lake water with a depth of 5 m is applied to the upper surface of this three-dimensional model as a uniform compressive stress of 5×10^4 Pa; the front, back, left, and right sides of this three-dimensional model are set as horizontal displacement constraints; the underside of this three-dimensional model is set as a fixed constraint.

The initial conditions of stress field are as follows: the initial stress of this three-dimensional model is calculated according to the self-weight stress of soil mass.

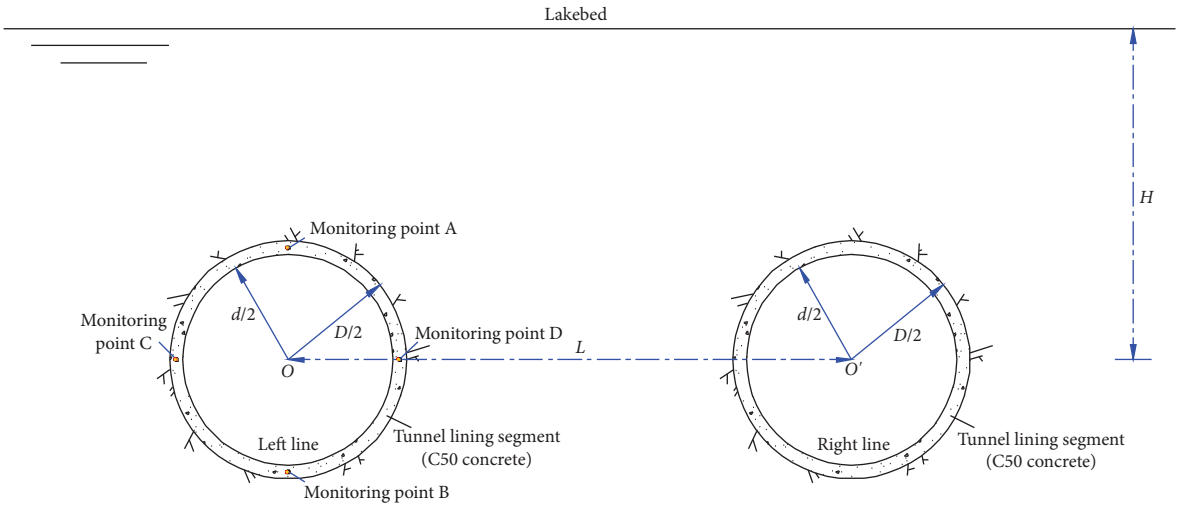

Figure 1: The cross-section sketch of special subway section passing through a lake.

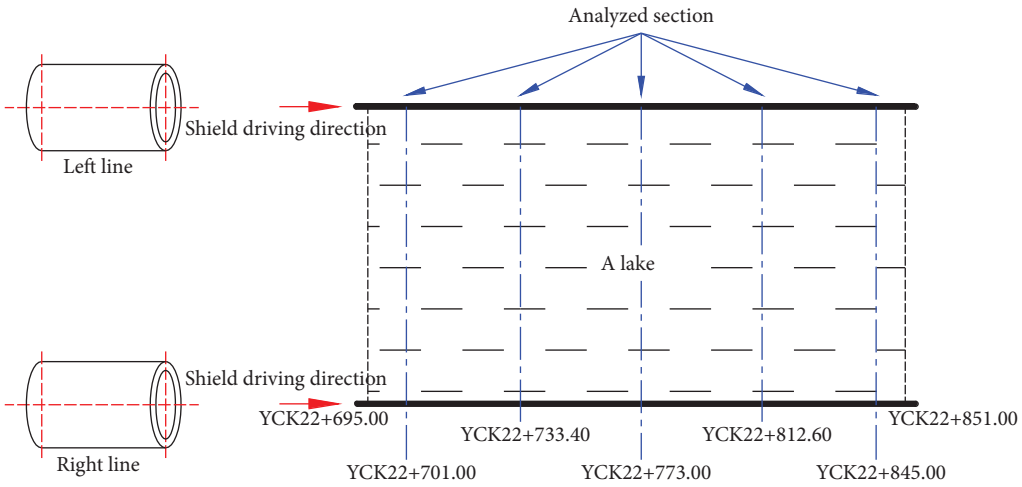

Figure 2: The plan sketch of special subway section passing through a lake.

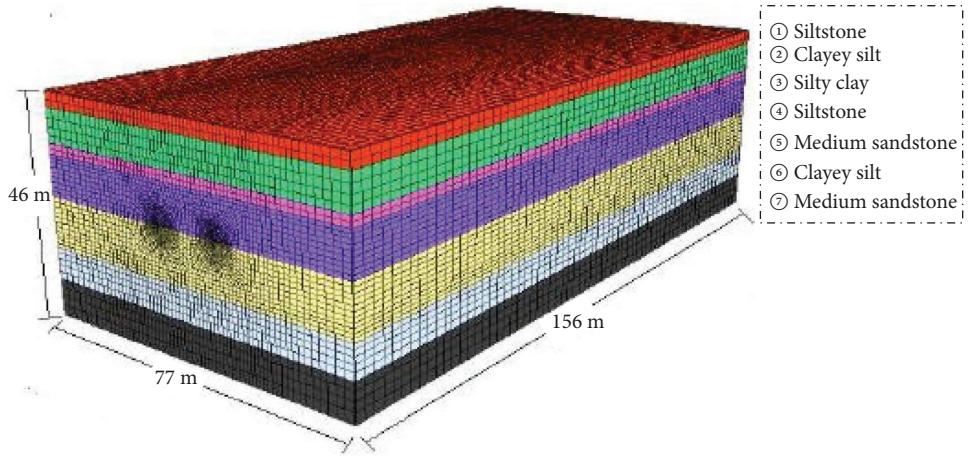

Figure 3: The establishment of three-dimensional model.

Table 1: The physical and mechanical parameters of soil mass in each layer.

Lithology types	Thickness (m)	Unit weight (kN/m^3)	Porosity	Permeability coefficient (m^2/Pa-sec)	Elasticity modulus (MPa)	Cohesion (kPa)	Internal friction angle (°)	Poisson's ratio
Siltstone	3.1	20.0	0.386	4.7×10^{-9}	12.0	6.8	35.8	0.25
Clayey silt	7.1	19.7	0.418	4.7×10^{-10}	9.3	10.9	17.9	0.31
Silty clay	2.2	19.3	0.456	8.3×10^{-11}	11.5	22.2	10.7	0.34
Siltstone	8.7	20.0	0.386	4.7×10^{-9}	12.0	6.8	35.8	0.25
Medium sandstone	10.5	20.4	0.363	1.4×10^{-8}	10.0	8.5	35.9	0.29
Clayey silt	6.7	19.8	0.418	5.9×10^{-10}	7.6	11.6	14.7	0.30
Medium sandstone	7.7	20.4	0.319	7.3×10^{-9}	10.1	13.6	32.6	0.28

The seepage boundary conditions of this three-dimensional model are as follows: a pore pressure of 5×10^4 Pa is applied to the upper surface of this three-dimensional model. For soft clay, its permeability coefficient is small. In the instantaneous deformation stage of shield tunnel construction, the external boundary of the model cannot be drained in time. Therefore, except for the upper surface, it is assumed that the left and right boundaries, front and back boundaries, bottom boundary, and tunnel boundary of the model are impermeable. However, in the long-term consolidation settlement development and change process of the tunnel, since the front and back boundaries, left and right boundaries, and bottom boundary of the model are far away from the tunnel, the pore water pressure here is set as the initial hydrostatic pressure value unchanged, so the front and back boundaries, left and right boundaries, and bottom boundary of the model are all permeable. During tunnel shield excavation, the pore water pressure at the inner boundary of the tunnel lining segment is fixed at 0.

The initial seepage conditions are as follows: the initial pore water pressure in the soil before tunnel excavation is the hydrostatic pressure in the rock soil layer.

First of all, remove the stratum element that needs to excavate the segment ring; at the same time, apply the segment element to simulate the support of the ring segment, apply the support stress on the excavation face, close the fluid seepage analysis part in FLAC^{3D}, calculate the deformation of the model in the undrained state of the soil in the single mechanical field, iterate to make the model balanced in the undrained state, and then open the fluid seepage field. The drainage deformation (consolidation deformation) of soil mass within the excavation time of this ring is calculated by fluid-solid coupling method. After the coupling calculation of this time step is completed, the next ring excavation process is calculated. The cycle is repeated until the tunnel excavation is completed. The program implementation of the shield tunnel excavation process is shown in Figure 4.

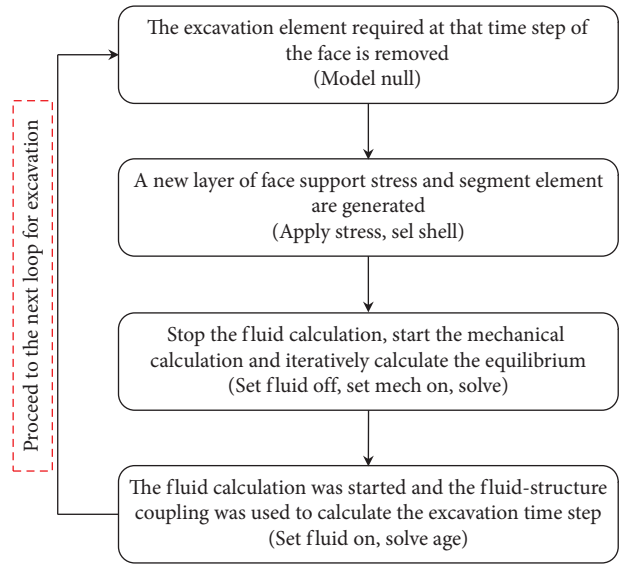

Figure 4: The program implementation of shield tunnel excavation process.

4.3. The Analysis of Numerical Simulation Results

4.3.1. The Analysis of Surrounding Rock Stress Field. Before the shield tunnel excavating, the rock and soil mass are in a state of stress balance as shown in Figure 5(a). After the shield tunnel excavating, due to the disturbance of shield tunnel construction and excavation, the stress balance state in the rock and soil mass changes, so that the stress field of surrounding rock is redistributed. The change of the stress field of the surrounding rock will change the permeability of rock and soil mass, and then the pore water pressure of surrounding rock changes accordingly. The change of pore water pressure will also affect the distribution of surrounding rock stress field, and the two interact and influence each other. Under the condition of fluid structure coupling, after a period of time, the stress field and seepage field finally reach a relative equilibrium state as shown in Figure 5(b).

During the excavation of left and right tunnels in turn, the vertical stress and horizontal stress of the surrounding rock at YCK22 + 701.00, YCK22 + 773.00 and YCK22 + 845.00 cross-sections were studied and analyzed, respectively. The vertical stress nephogram and horizontal stress nephogram of the tunnels and surrounding rock during the excavation of the left and right tunnels are shown in Figures 6 and 7, respectively.

According to Figure 6, it can be seen that during the shield tunneling on the left line, when the driving face

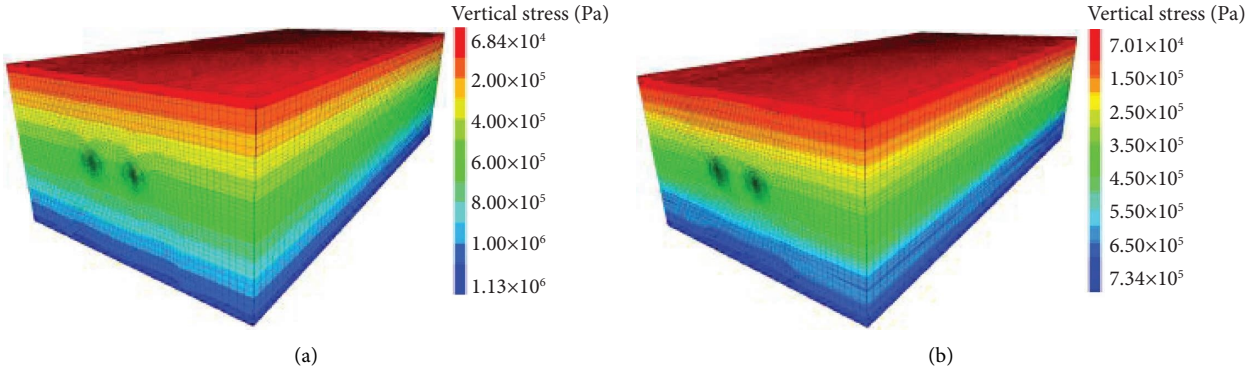

FIGURE 5: The vertical stress distribution of FLAC^{3D} numerical model. (a) Stress equilibrium state I (before shield tunneling) and (b) stress equilibrium state II (after shield tunneling).

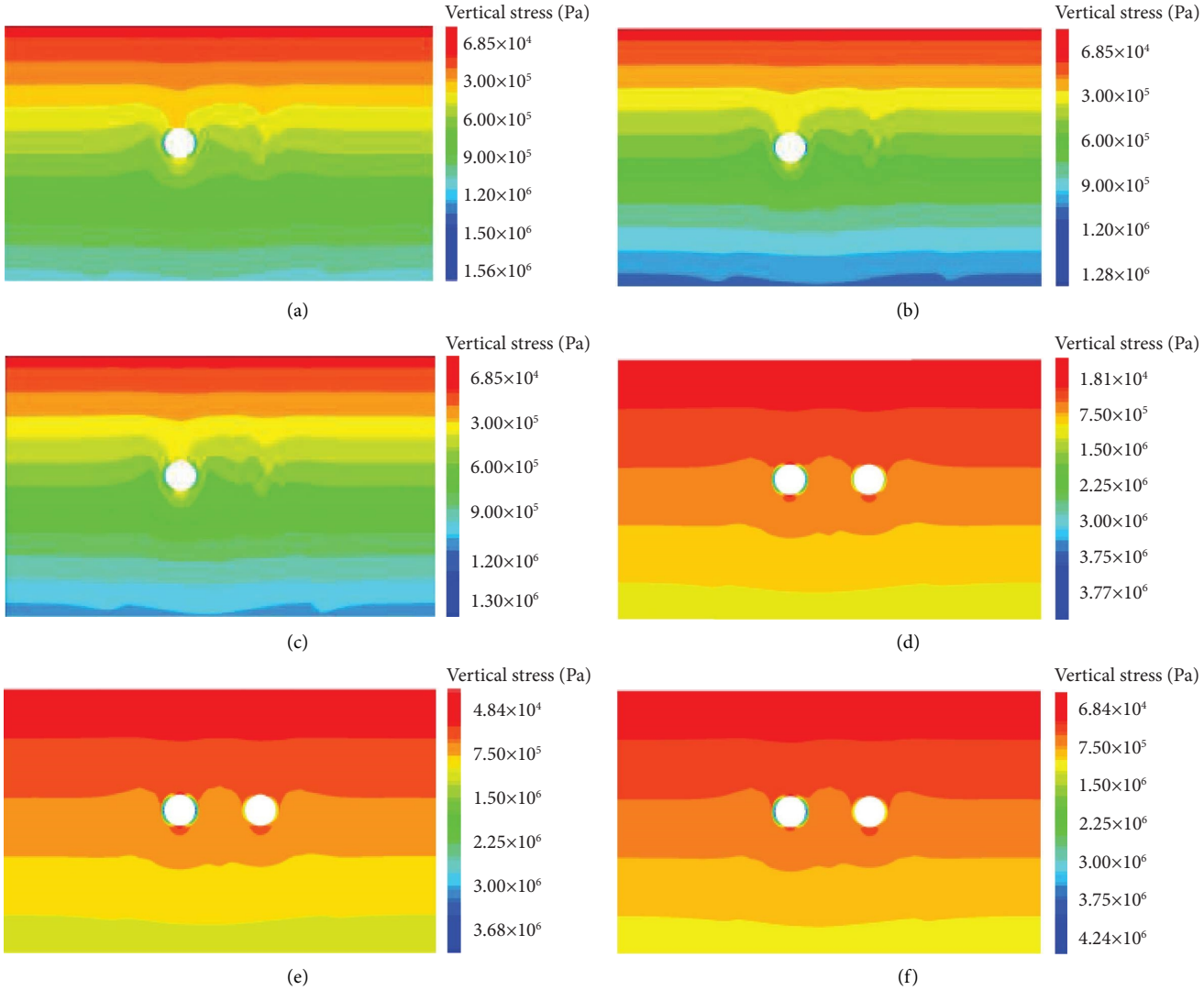

FIGURE 6: The vertical stress nephogram of the tunnels and surrounding rock. (a) YCK22 + 701.00 cross-section (left tunnel), (b) YCK22 + 773.00 cross-section (left tunnel), (c) YCK22 + 845.00 cross-section (left tunnel), (d) YCK22 + 701.00 cross-section (right tunnel), (e) YCK22 + 773.00 cross-section (right tunnel), and (f) YCK22 + 845.00 cross-section (right tunnel).

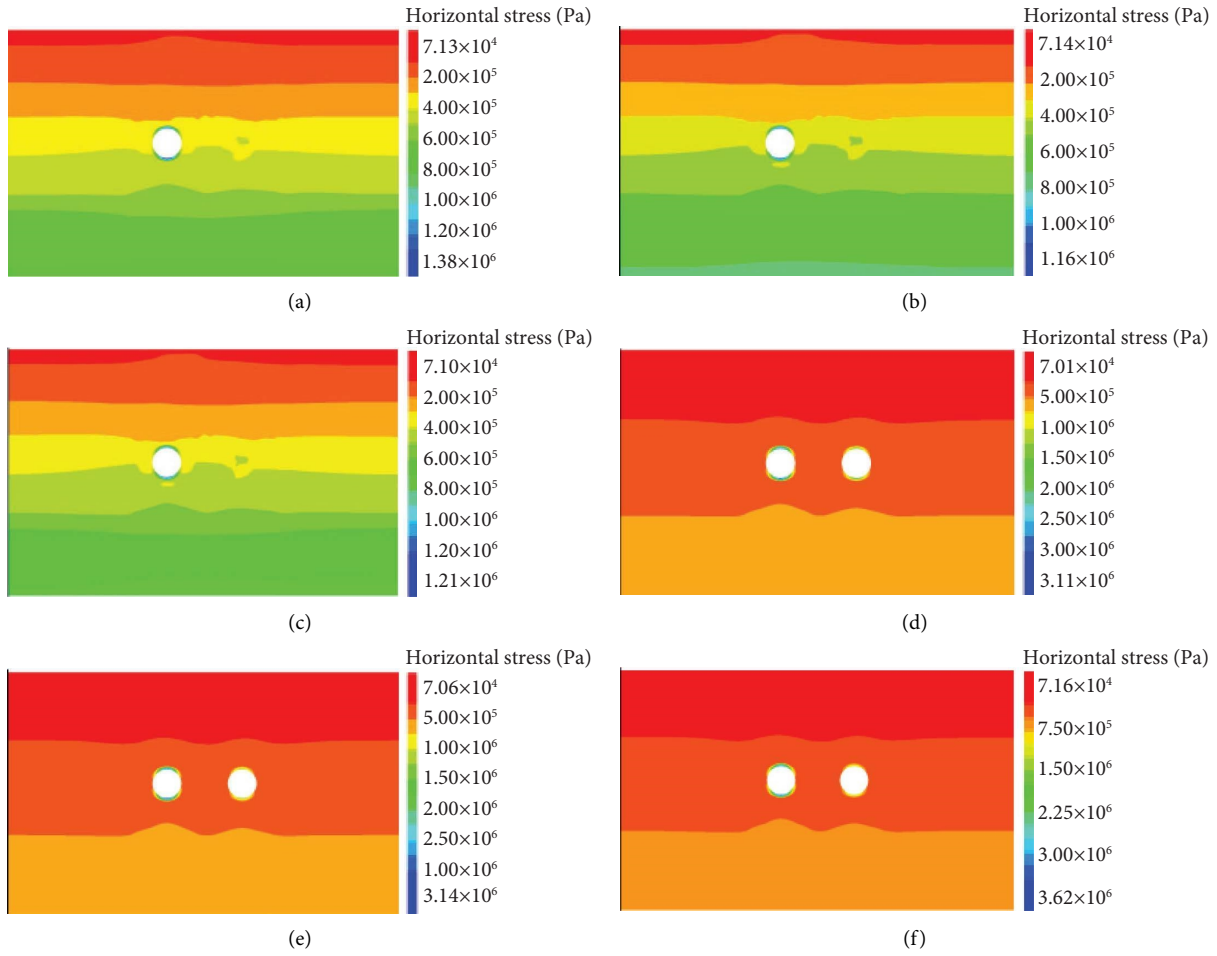

Figure 7: The horizontal stress nephogram of the tunnels and surrounding rock. (a) YCK22 + 701.00 cross-section (left tunnel), (b) YCK22 + 773.00 cross-section (left tunnel), (c) YCK22 + 845.00 cross-section (left tunnel), (d) YCK22 + 701.00 cross-section (right tunnel), (e) YCK22 + 773.00 cross-section (right tunnel), and (f) YCK22 + 845.00 cross-section (right tunnel).

advances to position of YCK22 + 701.00 cross-section, the maximum vertical effective stress of surrounding rock of left line is about 0.96 MPa; when the driving face advances to position of YCK22 + 773.00 cross-section, the maximum vertical effective stress of the surrounding rock of left line is about 1.33 MPa; and when the driving face advances to position of YCK22 + 845.00 cross-section, the maximum vertical effective stress of surrounding rock of left line is about 1.92 MPa. In the future, it can be seen that during the shield tunneling on the right line, it will cause static and dynamic load interference on the left line, and the maximum vertical effective stress of surrounding rock of left line will further increase. It can be seen that during the shield tunneling on the right line, when the driving face advances to position of YCK22 + 701.00 cross-section, the maximum vertical effective stress of surrounding rock of left line increases to 2.25 MPa and the maximum vertical effective stress of surrounding rock of right line is about 1.37 MPa; when the driving face advances to position of YCK22 + 773.00 cross-section, the maximum vertical effective stress of surrounding rock of left line increases to 3.72 MPa and the maximum vertical effective stress of surrounding rock of right line is about 1.86 MPa; when the driving face advances to position of YCK22 + 845.00 cross-section, the maximum vertical effective stress of surrounding rock of left line increases to 4.24 MPa and the maximum vertical effective stress of surrounding rock of right line is about 2.41 MPa. The maximum vertical effective stress of the surrounding rock of left and right lines is mainly concentrated at the arch foot position.

According to Figure 7, it can be seen that during the shield tunneling on the left line, when the driving face advances to position of YCK22 + 701.00 cross-section, the maximum horizontal effective stress of surrounding rock of left line is about 0.63 MPa; when the driving face advances to position of YCK22 + 773.00 cross-section, the maximum horizontal effective stress of surrounding rock of left line is about 1.14 MPa; and when the driving face advances to position of YCK22 + 845.00 cross-section, the maximum horizontal effective stress of surrounding rock of left line is about 1.66 MPa. In the future, it can be seen that during the shield tunneling on the right line, it will cause static and dynamic load interference on the left line, and the maximum horizontal effective stress of surrounding rock of left line will

further increase. It can be seen that during the shield tunneling on the right line, when the driving face advances to position of YCK22 + 701.00 cross-section, the maximum horizontal effective stress of surrounding rock of left line increases to 1.92 MPa and the maximum horizontal effective stress of surrounding rock of right line is about 0.97 MPa; and when the driving face advances to position of YCK22 + 773.00 cross-section, the maximum horizontal effective stress of surrounding rock of left line increases to 3.02 MPa and the maximum horizontal effective stress of surrounding rock of right line is about 1.53 MPa; when the driving face advances to position of YCK22 + 845.00 cross-section, the maximum horizontal effective stress of surrounding rock of left line increases to 3.61 MPa and the maximum horizontal effective stress of surrounding rock of right line is about 2.09 MPa. The maximum horizontal effective stress of surrounding rock of left and right lines is mainly concentrated on the side walls on both sides.

According to the numerical simulation results of vertical stress and horizontal stress nephograms in Figures 6 and 7, the following results can be obtained:

(1) Before shield tunneling, the vertical effective stress in the initial geostress field obtained by using the weight of rock and soil mass and horizontal effective stresses is symmetrically distributed.

(2) The stress field of the soil around the tunnel has become significant due to the combined influence of shield tunneling on the disturbance and seepage of the soil around the tunnel. During the construction of the left- and right-line shield tunnels successively excavating under the lake bottom, the vertical effective stress and horizontal effective stress of the arch crown and arch bottom of the left- and right-line tunnels increase with the gradual excavation of the shield machine. Especially when the right-line shield tunnel is excavated, the effective stress increases most significantly. During the excavation of the left-line shield tunnel, the vertical stress field forms a funnel-shaped distribution around the left-line tunnel, and during the excavation of the right-line shield tunnel, the vertical stress field forms a funnel-shaped distribution around the right tunnel. The two are symmetrically distributed with the central axis as the symmetrical center. The influence scope of the shield tunneling on the soil around the tunnel gradually expands with the shield tunneling.

(3) During the excavation of left and right tunnels in turn, the maximum vertical effective stress is about 4.24 MPa, which is mainly distributed at the arch foot of the tunnel. The maximum effective stress in the horizontal direction is about 3.61 MPa, which appears on both side walls of the tunnel in the horizontal direction.

4.3.2. The Analysis of Surrounding Rock Seepage Field. Disturbance to surrounding soil during shield tunneling is bound to change the permeability of soil, resulting in changes in fluid pore water pressure. Monitoring points are set at the vault, arch bottom, left arch waist, and right arch waist of the left-line tunnel of YCK22 + 773.00 cross-section, recorded as monitoring points A, B, C, and D (refer to Figure 1), and the pore water pressure at each monitoring point changes with the progress of tunnel excavation. The pore water pressure change curve is shown in Figure 8.

Figure 8 shows that the pore water pressure at each monitoring point basically remains unchanged before the excavation of the left-line tunnel is pushed to the YCK22 + 773.00 cross-section. After the excavation is pushed to the YCK22 + 773.00 cross-section, the pore water pressure at monitoring points A, C, and D first increases sharply (the corresponding peaks are 0.32 MPa, 0.31 MPa, and 0.30 MPa) and then drops abruptly and tends to be stable, while the pore water pressure at monitoring point B remains basically unchanged throughout the excavation process. The pore water pressure at monitoring point A decreases from about 0.23 MPa before excavation to about 0.2 MPa. The pore water pressure at monitoring point C decreases from about 0.26 MPa before excavation to about 0.035 MPa. The pore water pressure at monitoring point D decreases from about 0.26 MPa before excavation to about 0.038 MPa. The pore water pressure value at the monitoring points of the arch crown of each left-line tunnel decreases continuously, especially after the shield machine passes through the YCK22 + 773.00 cross-section, and the pore water pressure value at the monitoring points tends to be stable about 0.013 MPa after the left-line tunnel is completed. It can be seen that the shield tunneling has a great influence on the distribution of pore water pressure around the tunnel, and the pore water pressure around the tunnel after the completion of shield tunneling has a large drop compared with the initial pore water pressure.

Before the shield tunneling, the initial pore water pressure distribution is shown in Figure 9. The initial pore water pressure of the upper boundary of the model is 0.05 MPa, and the initial pore water pressure of the lower boundary of the model is 0.51 MPa. Due to the influence of shield tunneling, the stress field of soil mass is redistributed, which makes the original cracks in rock and soil mass further expand and new cracks are generated, and then the permeability of rock and soil mass changes. The variation of seepage field obtained at each excavation step under fluid structure coupling is shown in Figure 10.

Figure 10 shows that during the construction of the left-line shield tunnel, the pore water pressure distribution around the left-line tunnel has changed significantly compared with that before the construction. The pore water pressure of surrounding rock around the tunnel is significantly lower than the initial pore water pressure value. Driven by the hydraulic gradient, the groundwater begins to penetrate into the tunnel, and the groundwater at the far end flows to the excavation free face. Finally, a seepage field distribution shape similar to "precipitation funnel" is formed with the tunnel excavation area as the center. After the right-line tunnel is excavated, the pore water pressure of surrounding rock is symmetrically distributed with the central axis of the two tunnels as the symmetrical center; in

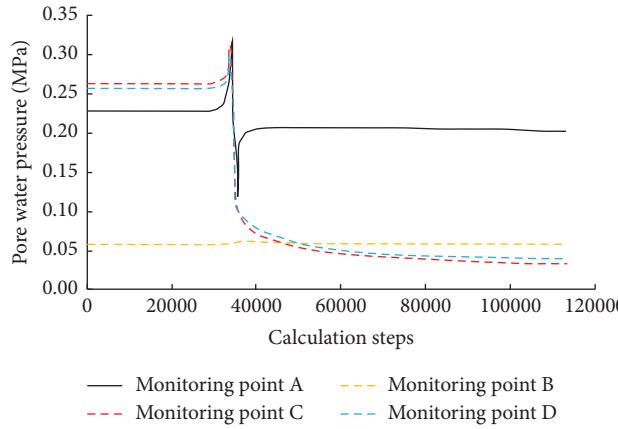

Figure 8: The change curves of pore water pressure at different monitoring points.

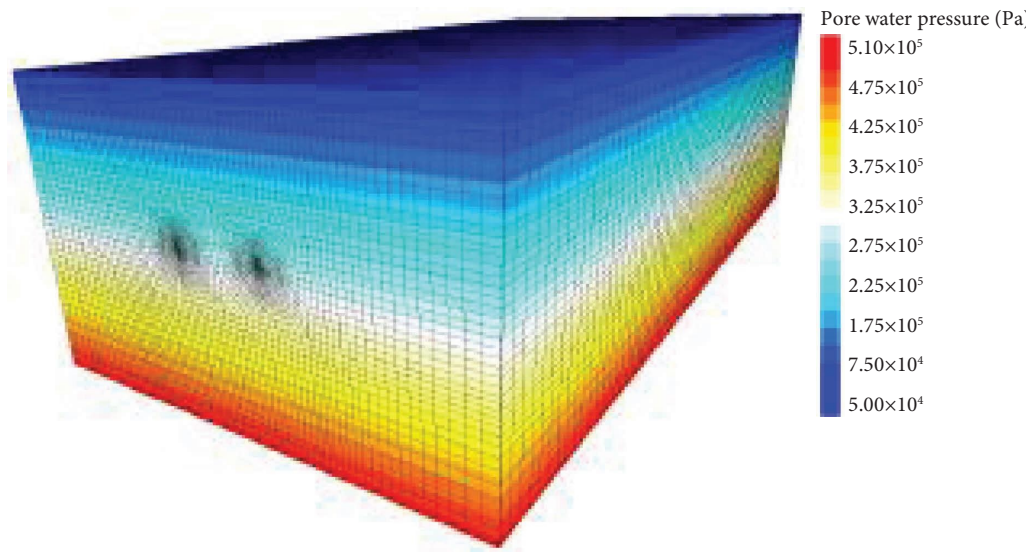

Figure 9: The initial pore water pressure distribution of FLAC^{3D} numerical model.

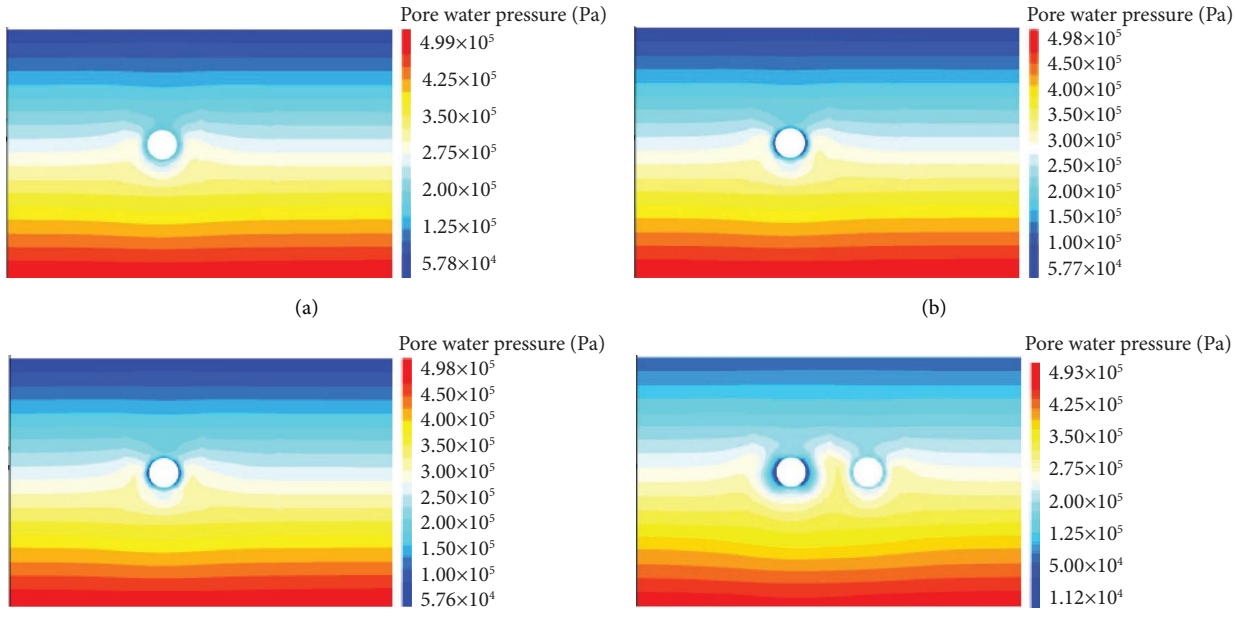

Figure 10: Continued.

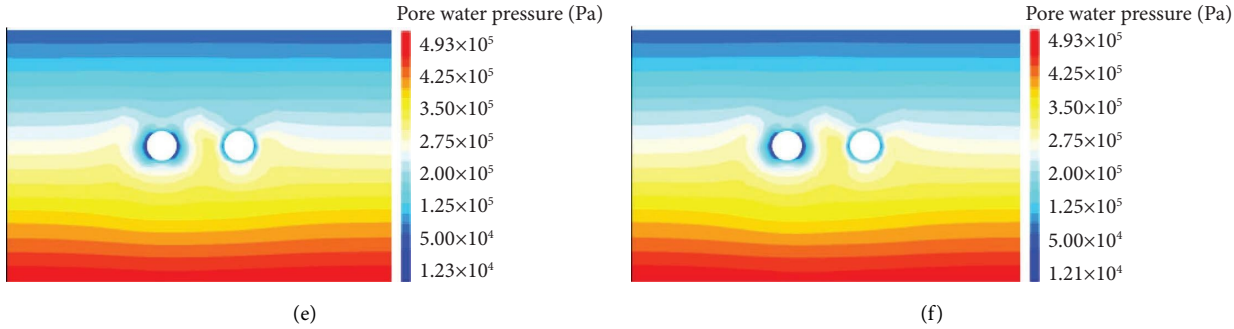

Figure 10: The pore water pressure nephogram of the tunnels and surrounding rock. (a) YCK22 + 701.00 cross-section (left tunnel), (b) YCK22 + 773.00 cross-section (left tunnel), (c) YCK22 + 845.00 cross-section (left tunnel), (d) YCK22 + 701.00 cross-section (right tunnel), (e) YCK22 + 773.00 cross-section (right tunnel), and (f) YCK22 + 845.00 cross-section (right tunnel).

the process of shield tunneling, the pore water pressure around the tunnel generally shows a downward trend, especially in the process of right-line tunnel excavation. The main reason is that the drainage boundary is larger when the right track tunnel is excavated, and more pore water is discharged at the same time.

After the asynchronous excavation of the left and right tunnels, the YCK22 + 773.00 cross-section is taken as the observation surface. The distribution of the flow vector of the groundwater seepage field around the tunnel is shown in Figure 11.

Figure 11 shows that the flow vector distribution on both sides of the tunnel arch waist is particularly concentrated, which is prone to water seepage. During the construction process, the water pressure changes on both sides of the tunnel arch waist shall be monitored, and the grouting behind the wall shall be carried out in time to avoid the formation of the water channel around the tunnel. At the same time, sufficient grease shall be injected at the shield tail brush to ensure the compactness of the shield tail and prevent the shield tail from being punctured.

4.3.3. The Analysis of Surrounding Rock Displacement Field. Similarly, the vertical displacement of soil mass is recorded at monitoring point A and monitoring point B, and the horizontal displacement of soil mass is recorded at monitoring point C and monitoring point D as shown in Figure 12.

Figure 12 shows that when the tunnel is excavated to YCK22 + 773.00 cross-section, the soil at the tunnel arch crown suddenly subsides, the soil at the arch bottom suddenly rises, and the soil on both sides of the tunnel arch waist moves away from the tunnel. After shield tunnel excavation, due to the change of stress release and pore water pressure on the excavation surface with different excavation footage, the surrounding rock will have different displacement in different construction stages. The vertical displacement nephogram in each construction stage is shown in Figure 13.

Figure 13 shows that during the lake bottom excavation of the left line shield tunnel, a large settlement displacement occurred at the tunnel arch crown, with the maximum value of about 20.19 mm; a large uplift displacement occurred at the arch bottom of the tunnel, with the maximum value of 21.72 mm. The scope of influence on the displacement field during the excavation of the left-line shield tunnel gradually expands to the bottom of the lake with the advance of excavation and expands to both sides in a funnel shape above the left tunnel. The displacement is gradually weakened from the tunnel section to the upper and lower directions. When the right-line shield tunnel starts excavation, its displacement field impact is similar to that of the left tunnel excavation, and the impact area gradually expands to the bottom of the lake with the advance of excavation, which is funneled to both sides above the left tunnel, roughly symmetrical to the impact area above the left tunnel, and produces superimposed impact in the middle area, and the displacement size gradually decreases from the tunnel section to the upper and lower directions. The maximum vertical settlement displacement during the whole excavation process is about 24.09 mm, and the maximum uplift displacement is about 25.28 mm. According to the corresponding standards (GB/T 51438-2021, standard for design of shield tunnel engineering), it can be seen that the maximum displacement of surrounding rock of left or right line should not exceed 20 mm. However, the on-site numerical simulation monitoring results are all greater than 20 mm; therefore, it is necessary to adopt methods such as pregrouting to reinforce the soil and prevent excessive deformation of the surrounding rock during shield tunneling.

4.3.4. The Analysis of Lining Segment Displacement Field. According to the plan sketch of a special subway section passing through a lake in Figure 2, the lining segment installed at YCK22 + 773.00 cross-section (left tunnel) is taken as the research object. The horizontal and vertical displacement nephogram of this lining segment after its splicing are shown in Figure 14.

The horizontal and vertical displacement nephogram of this lining segment after the left-line excavation is completed is shown in Figure 15.

The horizontal and vertical displacement nephogram of this lining segment after the right line is excavated to YCK22 + 773.00 cross-section is shown in Figure 16.

The horizontal and vertical displacement nephogram of this lining segment after the right-line excavation is completed is shown in Figure 17.

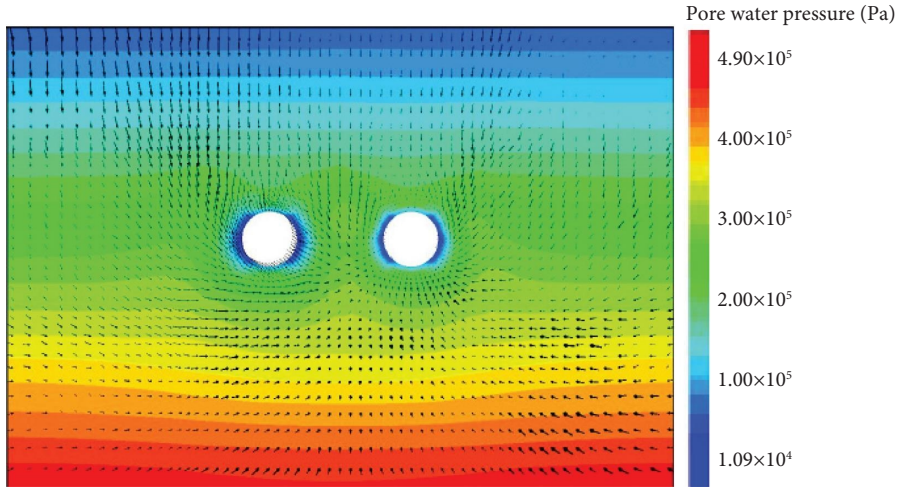

Figure 11: The pore water pressure nephogram and corresponding flow vector of the tunnels and surrounding rock.

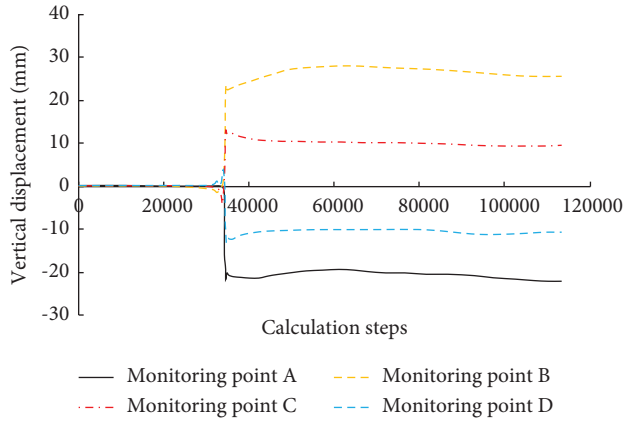

Figure 12: The change curves of vertical displacement at different monitoring points.

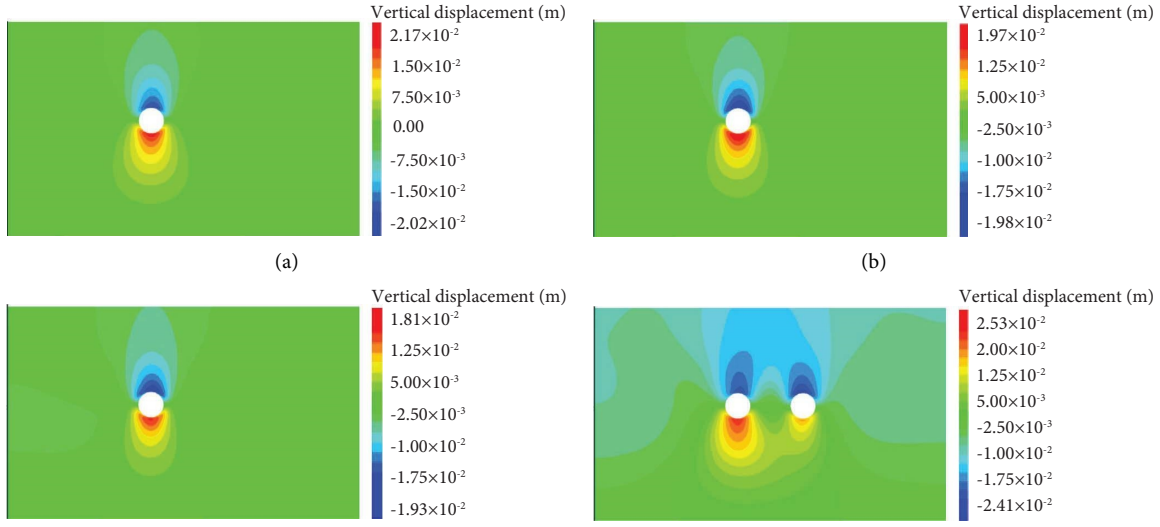

Figure 13: Continued.

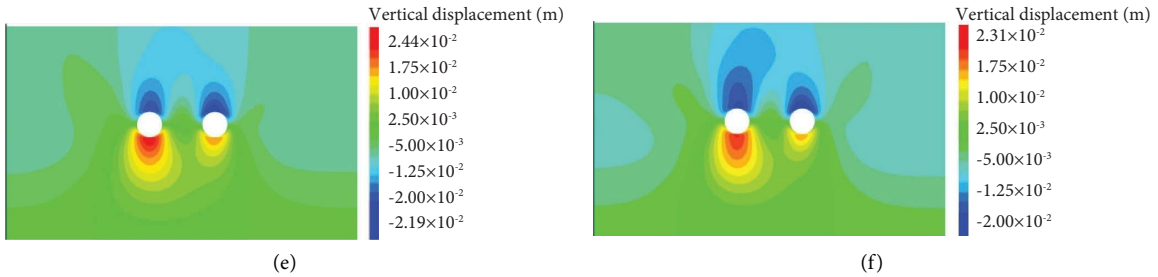

Figure 13: The vertical displacement nephogram of the tunnels and surrounding rock. (a) YCK22 + 701.00 cross-section (left tunnel), (b) YCK22 + 773.00 cross-section (left tunnel), (c) YCK22 + 845.00 cross-section (left tunnel), (d) YCK22 + 701.00 cross-section (right tunnel), (e) YCK22 + 773.00 cross-section (right tunnel), and (f) YCK22 + 845.00 cross-section (right tunnel).

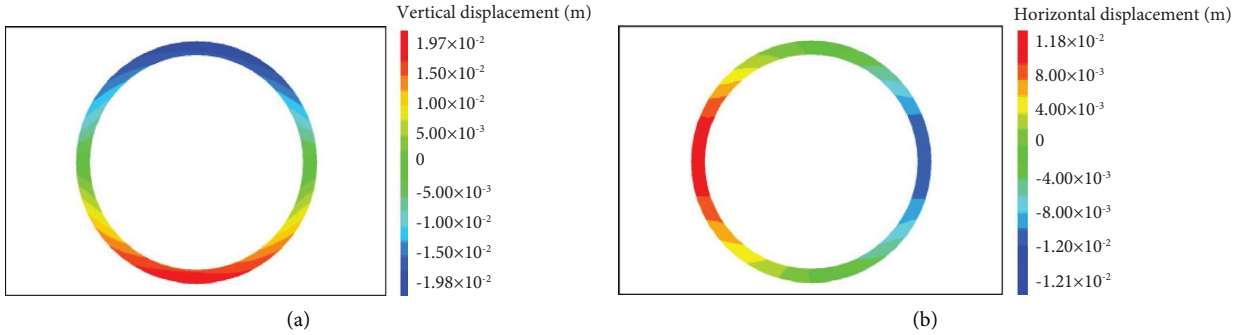

Figure 14: The displacement nephogram of lining segment installed at YCK22 + 773.00 cross-section (left tunnel). (a) Horizontal displacement after it splicing and (b) vertical displacement after it splicing.

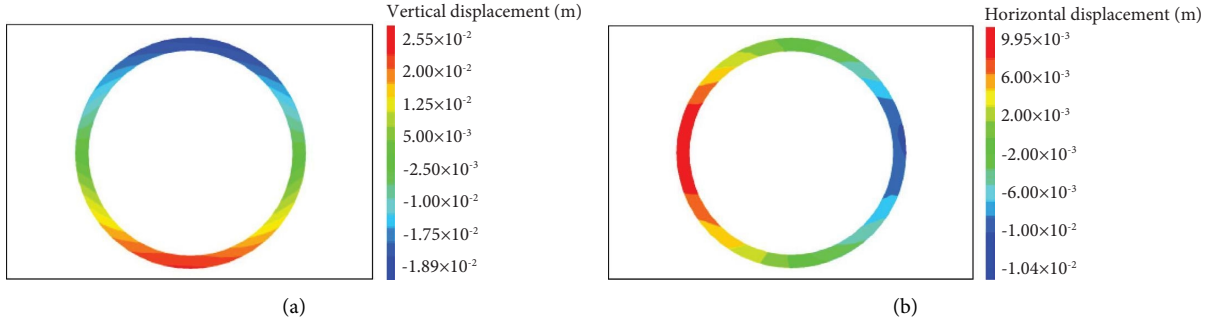

Figure 15: The displacement nephogram of lining segment installed at YCK22 + 773.00 cross-section (left tunnel). (a) Horizontal displacement after the left-line excavation is completed and (b) vertical displacement after the left-line excavation is completed.

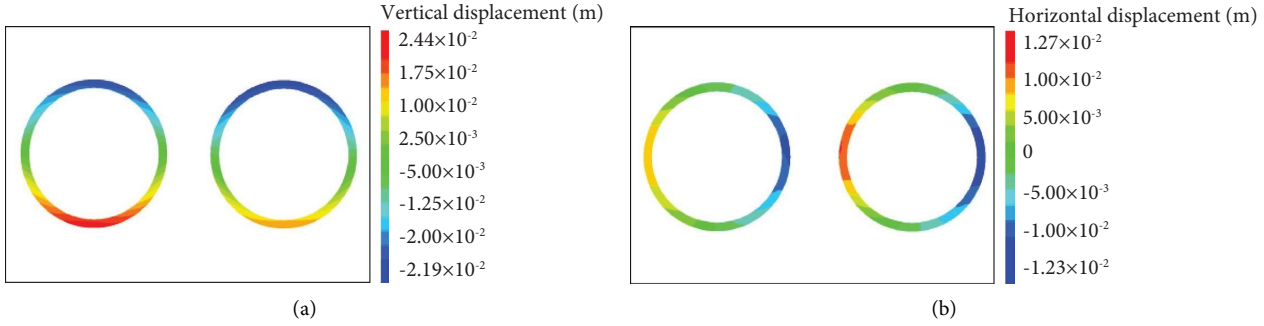

Figure 16: The displacement nephogram of lining segment installed at YCK22 + 773.00 cross-section (left tunnel). (a) Horizontal displacement after the right line is excavated to YCK22 + 773.00 cross-section and (b) vertical displacement after the right line is excavated to YCK22 + 773.00 cross-section.

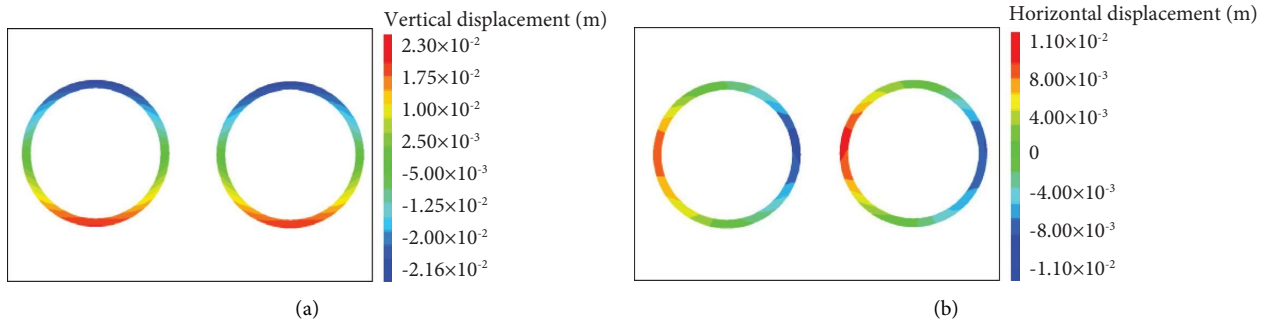

Figure 17: The displacement nephogram of lining segment installed at YCK22 + 773.00 cross-section (left tunnel). (a) Horizontal displacement after the right-line excavation is completed and (b) vertical displacement after the right-line excavation is completed.

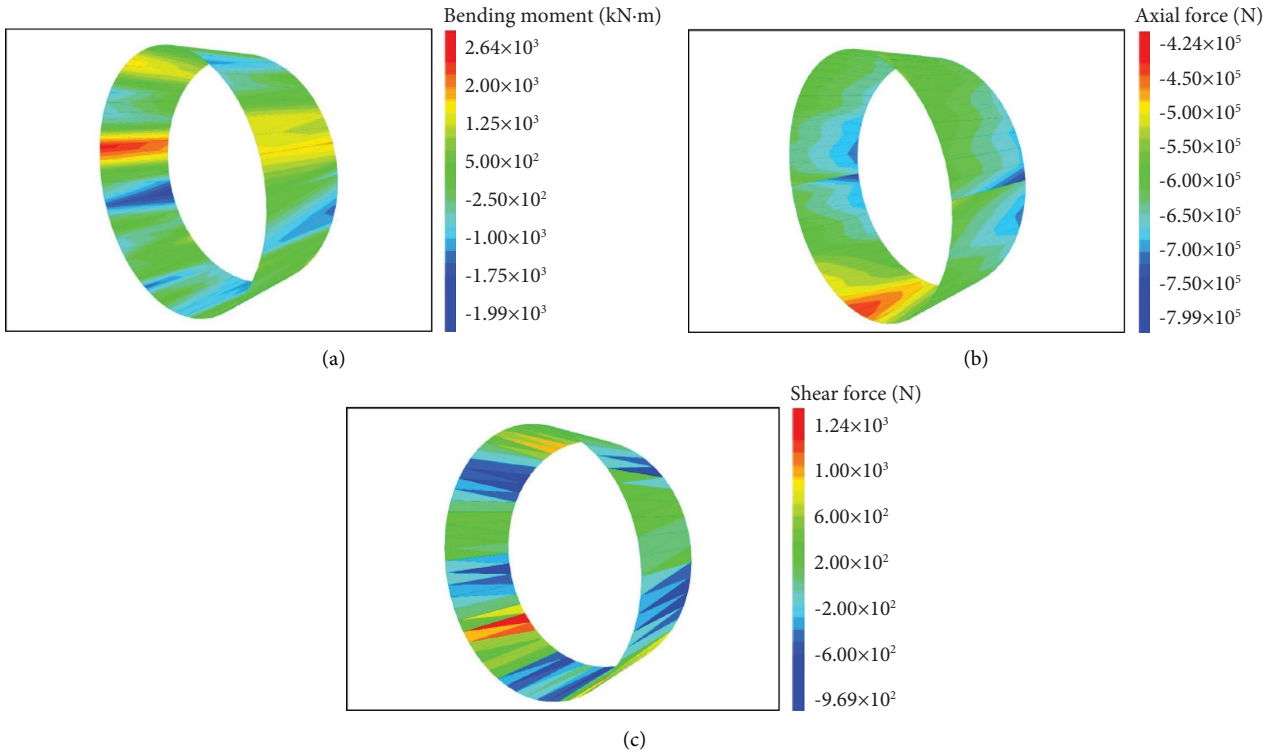

Figure 18: The internal force nephogram of lining segment installed at YCK22 + 773.00 cross-section (left tunnel). (a) Bending moment after the left-line excavation is completed, (b) axial force after the left-line excavation is completed, and (c) shear force after the left-line excavation is completed.

Figures 14–17 show that the vertical displacement of lining segment installed at YCK22 + 773.00 cross-section (left tunnel) increases gradually with the increase of the excavation step after the completion of the splicing. The vertical displacement reaches the maximum after the completion of the excavation of the left-line tunnel, starts to decline, and tends to be stable during the excavation of the right-line tunnel. The segment vault has settlement, the maximum settlement is 21.8 mm, and the arch bottom has uplift, the maximum uplift is 24.4 mm. The maximum horizontal displacement of the segment appears on both sides of the arch waist, and the maximum horizontal displacement value gradually decreases with the increase of the excavation step. When the right-line tunnel is excavated, the left displacement value of the lining segment installed at YCK22 + 773.00 cross-section (left tunnel) continuously decreases, and the right displacement value of the lining segment has no obvious change. According to the corresponding standards (GB/T 51438-2021, standard for design of shield tunnel engineering), it can be seen that the maximum displacement of lining segment of left or right line should not exceed 1/300 of the lining segment, and the calculation shows that it is about 20.6 mm. However, the on-site numerical simulation monitoring results are all greater than 20.6 mm; therefore, it is also necessary to adopt methods such as grouting to reinforce the soil and prevent excessive deformation of the lining segment during shield tunneling.

4.3.5. The Analysis of Lining Segment Internal Force Field. The bending moment, axial force, and shear force nephogram of the lining segment installed at YCK22 + 773.00 cross-section (left tunnel) after the left-line excavation is completed are shown in Figure 18.

Figure 18 shows that the positive bending moment of the lining segment is mainly distributed on both sides of the arch crown, and the negative bending moment is mainly distributed on both sides of the arch bottom. The axial force of the lining segment is compressive stress, and the maximum axial force is mainly distributed on both sides of the arch waist. The maximum normal shear stress occurs on both sides of the segment arch bottom.

5. Conclusions

(1) With the rapid development of the economy and the great progress of science and technology, underwater tunnel construction technology has also made great progress. At present, underwater tunnel has gradually become an important means of transportation across rivers, lakes, and seas at home and abroad. Different from other tunnels, the geological conditions and internal and external environment of underwater tunnels are generally complex. If disasters occur during the operation period, it is easy to cause significant economic losses and adverse social impacts.

(2) Based on the coupling theory of seepage field and stress field, the equations of seepage field and stress field coupling are derived, which provides theoretical support for the follow-up research on the fluid structure coupling problem of the underwater shield tunnel and numerical simulation.

(3) During the excavation of left and right tunnels in turn, the maximum vertical effective stress is about 4.24 MPa, which occurs at the arch foot of the tunnel. The maximum effective stress in the horizontal direction is about 3.61 MPa, which appears on both side walls of the tunnel in the horizontal direction.

(4) During the excavation of the left-line shield tunnel, the surrounding rock pore water pressure distribution forms a seepage field distribution shape similar to a "precipitation funnel" with the tunnel excavation area as the center, and the surrounding rock seepage field distribution is symmetrical after the excavation of the right-line tunnel. Also, the flow vector distribution on both sides of the tunnel arch waist is particularly concentrated, which is prone to water seepage. During the construction, the water pressure changes on both sides of the tunnel arch waist should be monitored.

(5) The compressive stress of the lining segment is mainly distributed on both sides of the arch waist and the arch bottom of the lining segment, without the generation of tensile stress. The tensile stress is mainly distributed at the arch crown and the arch bottom of the lining segment. The arch crown of the lining segment is subject to settlement, and the arch bottom is subject to uplift. The maximum horizontal displacement is mainly distributed on both sides of the arch waist of the lining segment, and the lining segment converges inward as a whole.

Data Availability

All data used to support the findings of this study are included within the article, and there are no restrictions on data access.

Conflicts of Interest

The authors declare that they have no conflicts of interest.

Authors' Contributions

Zengqiang Yang was responsible for thesis writing and modification. Xiaoming You was responsible for some experiments and data processing. Huiwu Jin was responsible for thesis typesetting.

Acknowledgments

This work was supported by the China Postdoctoral Science Foundation (2023M732969), the National Natural Science Foundation of China project (52104091), the excellent teaching team of "Qinglan Project" in Jiangsu Universities, "Innovative Teaching Team of Road and Bridge Engineering Technology Specialty" (Teacher Letter Su (2021) no. 11), and the General project of the Chongqing Natural Science Foundation "structural safety research of large city underwater shield tunnel" (cstc2020jcyj-msxmx0846).

References

[1] D. Y. Ming, Y. D. Zhao, S. F. Wang, and Z. Q. Zhu, "Analysis of reasonable seepage mode of underwater shallow buried no-pressure circular tunnel lining," *Engineering Journal of Wuhan University*, vol. 54, no. 4, pp. 283–289, 2021.

[2] M. Deng, Z. Z. Zhang, W. J. Yu, J. L. Xin, and S. Q. Xu, "Acoustic emission characteristics and damage law for prefabricated single-crack sandstone under uniaxial compression," *Structural Control and Health Monitoring*, vol. 29, no. 10, pp. 1–16, 2022.

[3] Z. G. Du, J. L. Mei, Y. D. Ni, Y. F. Chen, and Z. N. Tang, "Review on evaluation and optimization of light environment of extra-long urban underwater tunnel based on visual demands," *Journal of Traffic and Transportation Engineering*, vol. 20, no. 6, pp. 48–61, 2020.

[4] Y. Yang, "Evaluation of potential hazard of underwater tunnel construction safety of Shenzhen-Zhongshan link based on mutation theory," *Tunnel Construction*, vol. 40, no. S1, pp. 75–81, 2020.

[5] L. Tang and H. Y. Guan, "Intelligent method of determining dimension of mortise and tenon joint based on parameterization," *Journal of Beijing Forestry University*, vol. 43, no. 3, pp. 145–154, 2021.

[6] Z. Z. Zhang, M. Deng, J. B. Bai, S. Yan, and X. Y. Yu, "Stability control of gob-side entry retained under the gob with close distance coal seams," *International Journal of Mining Science and Technology*, vol. 31, no. 2, pp. 321–332, 2021.

[7] S. T. Yang, Y. Lu, Y. Y. He, T. T. Liu, and X. Z. Ma, "Analysis of pore structure characteristics and seepage simulation of turfy soil based on CT scans," *Journal of Engineering Geology*, vol. 29, no. 5, pp. 1354–1365, 2021.

[8] Z. Q. Yang, C. Liu, G. A. Wang, G. W. Li, and F. S. Li, "Structural characteristics analysis of overlying rocks and prevention measures with a long-wall face passing across abandoned roadways: a case study," *Shock and Vibration*, vol. 2021, Article ID 6665341, 15 pages, 2021.

[9] J. Y. Peng, J. F. Zhang, Z. Z. Shen, and J. B. Ye, "Effect of grain shape on pore characteristics and permeability of coarse-grained soil," *Rock and Soil Mechanics*, vol. 41, no. 2, pp. 592–600, 2020.

[10] X. Feng, X. Peng, L. X. Li et al., "Influence of reservoir heterogeneity on water invasion differentiation in carbonate gas reservoirs," *Natural Gas Industry B*, vol. 6, no. 1, pp. 7–15, 2019.

[11] Y. S. Zhao, Z. C. Feng, and Z. J. Wan, "Least energy principle of dynamical failure of rock mass," *Chinese Journal of Rock Mechanics and Engineering*, vol. 22, no. 11, pp. 1781–1783, 2003.

[12] A. Lurka, "Location of high seismic activity zones and seismic hazard assessment in Zabrze Bielszowice coal mine using passive tomography," *Journal of China University of Mining and Technology*, vol. 18, no. 2, pp. 177–181, 2008.

[13] G. C. Zhang, L. J. Chen, Z. J. Wen et al., "Squeezing failure behavior of roof-coal masses in a gob-side entry driven under unstable overlying strata," *Energy Science and Engineering*, vol. 8, no. 7, pp. 2443–2456, 2020.

[14] S. H. Tang, X. P. Zhang, H. Liu et al., "Engineering dificulties and key technologies for undervater shield tunnel in complex ground," *Journal of Engineering Geology*, vol. 29, no. 5, pp. 1477–1487, 2021.

[15] W. J. Hu, J. Wang, and H. Ma, "Application of comprehensive advanced geological forecast in the tunnel engineering for the line two of west-east natural gas transmission project," *Natural Gas Industry*, vol. 30, no. 5, pp. 87–91, 2010.

[16] W. C. Fan, Z. C. Sun, F. Y. Li et al., "Research on prediction of tunneling parameters of super-large diameter slurry shield in composite strata of Shantou Bay Tunnel," *Tunnel Construction*, vol. 40, no. 8, pp. 1160–1168, 2020.

[17] N. N. Feng, "Research on influence of grouting rate of the shield tunnel on the stratum settlement," *Subgrade Engineering*, vol. 5, pp. 118–128, 2017.

[18] S. J. Zhang, R. T. Liu, S. C. Li, L. Z. Zhang, and P. Jiang, "Experimental study on ground surface heave affected by grouting in sandy soil layer," *Chinese Journal of Underground Space and Engineering*, vol. 14, no. 4, pp. 1097–1104, 2018.

[19] X. L. Liu, Q. H. Li, and Z. Q. Liao, "Investigation on wave-induced seabed response around a buried pipeline considering coupling effect of pore pressure accumulation and stresses," *Journal of Engineering Geology*, vol. 29, no. 6, pp. 1770–1778, 2021.

[20] J. H. Ye, D. S. Jeng, R. Wang, and C. Q. Zhu, "Numerical simulation of the wave-induced dynamic response of poro-elastoplastic seabed foundations and a composite breakwater," *Applied Mathematical Modelling*, vol. 39, no. 1, pp. 322–347, 2015.

[21] W. Cai, L. M. Dou, G. Y. Si, and Y. W. Hu, "Fault-induced coal burst mechanism under mining-induced static and dynamic stresses," *Engineering*, vol. 7, no. 5, pp. 687–700, 2021.

[22] Y. Wang, Y. C. Tao, K. Cheng, and Q. Yang, "Arbitrary resolved-unresolved CFD-DEM coupling method and its application to seepage flow analysis in sandy soil," *Chinese Journal of Geotechnical Engineering*, vol. 43, no. 11, pp. 2084–2093, 2021.

[23] T. B. Anderson and R. Jackson, "Fluid mechanical description of fluidized beds. equations of motion," *Industrial and Engineering Chemistry Fundamentals*, vol. 6, no. 4, pp. 527–539, 1967.

[24] Z. W. Deng, Z. Z. Wu, H. Cao, and P. H. Shen, "Surface deformation of slurry shield tunneling using fluid-solid coupling theory," *Journal of Central South University*, vol. 44, no. 2, pp. 785–791, 2013.